The multicritical region of the Gd - Lu alloy system

1996 J. Phys.: Condens. Matter 8 3661

(http://iopscience.iop.org/0953-8984/8/20/012)

J. Phys.: Condens. Matter **8** (1996) 3661–3670. Printed in the UK

The multicritical region of the Gd–Lu alloy system

R S Eccleston†, M L Vrtis‡, S B Palmer§, G J McIntyre‡ and D Fort‖

† Rutherford Appleton Laboratory, Chilton, Didcot, Oxon OX11 0QX, UK
‡ Institut Laue–Langevin, Centre de Tri, Avenue des Martyrs, Grenoble Cédex, France
§ Department of Physics, University of Warwick, Coventry CV4 7AL, UK
‖ School of Metallurgy and Materials, University of Birmingham, Birmingham B15 2TT, UK

Received 8 November 1995, in final form 29 January 1996

Abstract. The magnetic phase diagram of the Gd–Lu alloy system has been studied in the multicritical region using ultrasound velocity and attenuation measurements and neutron diffraction. A phase diagram has been drawn up on the basis of these measurements. The phase diagram has much in common with that of Gd–Y including the existence of a ferro I phase in which a net *c*-axis moment coexists with a paramagnetic distribution of spins in the basal plane. For Lu concentrations greater than 23.5% a helical antiferromagnetic (HAF) phase exists. At low temperatures all of the samples studied exhibit a canted ferromagnetic structure. The HAF-to-canted-ferromagnetic transition occurs when the pitch of the helix approaches zero and there is a small temperature range (≈2 K) over which canted ferromagnetic and HAF domains coexist.

1. Introduction

Gadolinium is unique amongst the rare earths in two respects: its 4f charge cloud is spherically symmetric, and consequently crystal-field interactions play no role in the magnetic ordering, and it is the only rare earth that does not exhibit a modulated antiferromagnetic structure at any temperature. Below a Curie temperature of 293 K it is a *c*-axis ferromagnet; the spins do, however, deviate from the *c*-axis by up to 15° [1]. At approximately 235 K the spins rotate away from the *c*-axis to form a canted ferromagnetic structure. The ferromagnetic phases owe their origins to two competing types of two-ion anisotropy. Gadolinium has a c/a ratio of 1.59, somewhat smaller than the ideal for the hexagonal close-packed structure of $\sqrt{8/3}$, and, as a consequence, the dipole–dipole interaction has an anisotropic contribution along the *c*-axis [2]. Another competing anisotropy which gains pre-eminence at lower temperatures stems from spin–orbit coupling to the conduction electrons [3], and favours a canted ferromagnetic structure.

The absence of helical order is attributed to the absence of nesting in the hole Fermi surface of Gd. Positron annihilation experiments [4] revealed a webbing which may join the 'toes' on the hole Fermi surface in all of the heavy rare earths except Gd. These parallel or nesting regions of the Fermi surface tend to produce peaks in the conduction electron susceptibility, $\chi(q)$ [5], which stabilize a periodic magnetic structure such as a helix. The non-magnetic impurities Y, Sc and Lu have the webbing feature in their Fermi surfaces, and when alloyed with Gd, even in relatively small amounts, the effect is strong enough to 'persuade' the Gd spins to order helically.

The magnetic phase diagram of the Gd–Y alloy system has been studied extensively by a variety of probes and the phase diagram is now well known [6]. Three phases of

0953-8984/96/203661+10$19.50

magnetic order have been observed in zero magnetic field: ferro I, ferro II and helical antiferromagnetic (HAF). Ferro I is akin to the high-temperature phase of Gd, displaying a net c-axis moment with apparent paramagnetism in the basal plane. There remains some doubt about the magnetic structure in the ferro I phase with two models describing the available experimental data reasonably well. The random-cone model [7] has the spins confined to the surface of a cone with a fixed semi-cone angle with the c-axis, but free to move round the surface of the cone. The virtual-crystal model [8] relies upon the break-up of long-range order by the statistical distribution of the diluent atoms which would leave spins which are dominated by Gd neighbours ordered along the c-axis and spins dominated by Y neighbours paramagnetic. Ferro II is a canted ferromagnetic structure like the low-temperature structure exhibited by Gd. For Y concentrations between 36% and 30%, as the temperature decreases the magnetic structure is first ferro I, then HAF and finally ferro II. Clearly in this region the magnetic structure is governed by the interplay of three competing interactions. The transition from HAF to ferro II actually involves two processes: (i) the turn angle of the helix becomes zero; and (ii) the spins lift out of the basal plane to form the canted ferromagnetic, ferro II, structure. There is no reason for which these two processes should occur simultaneously. Indeed some effort has already been devoted to trying to understand this transition.

The motivation for the study of Gd–Sc and Gd–Lu alloys stems from the reliance of the anisotropic interactions upon the c/a ratio, and also the belief that increasing the mismatch between diluent and lattice may reduce the long-range interaction by increasing scattering of conduction electrons, and favour a phase with a disordered component. The Gd–Sc system has been studied [9], and the phase diagram shows considerable differences from that of Gd–Y. Lu has an atomic radius between that of Y and Sc and as such it was hoped that it would provide an intermediate step between Gd–Y and Gd–Sc. The phase diagram of Gd–Lu, derived from bulk measurements, appears to show a great deal of similarity to that of Gd–Y. In this study, and in previous work published elsewhere [10], we have endeavoured to add more detail to the phase diagram and, by acquiring the microscopic information made available by a neutron diffraction measurement, shed more light on the nature of the ferro II–HAF phase transition, and on the existence and structure of the ferro I phase.

2. Experimental procedure

All of the crystals studied were grown at the School of Metallurgy and Materials, University of Birmingham, using a solid-state annealing technique [11].

Ultrasound measurements were performed in pulse echo mode on an automated system described elsewhere [12]. All measurements were made at a frequency of 15 MHz using quartz transducers bonded to the sample with epoxy resin. Bearing in mind the qualitative nature of the analysis of the ultrasound data, no corrections for sidewall reflections, aparallelism or attenuation at the transducer–sample interface were performed. The sample temperature was controlled by means of a standard continuous-flow cryostat with a temperature controller. Warming and cooling rates were approximately 0.2 K min^{-1}.

The neutron diffraction measurements were performed on the D9 diffractometer at the Institut Laue-Langevin, Grenoble. The high absorption cross section of both naturally occurring Gd and Lu for thermal neutrons precipitated the use of hot neutrons of wavelength 0.48 Å, below the absorption resonances of both elements. The crystal was mounted with the a^*- and c^*-directions in the basal plane, thereby optimizing resolution for scans of the $h0l$ type. D9 is equipped with a Displex closed-cycle refrigerator which operates at temperatures down to 15 K. Temperature readings were believed to be accurate to within

±0.5 K. Secondary nuclear extinction and absorption corrections were performed at the ILL using the UPALS and DATAP programs respectively. Magnetic extinction corrections were performed using a bespoke program which assumed magnetic domains to be of similar size to the mosaic blocks of the crystal.

3. Results and discussion

3.1. Ultrasonic measurements

We measured three elastic moduli, C_{33}, C_{44} and C_{11}, and their associated attenuation coefficients, α_{ij}, for $Gd_{76.0}Lu_{24.0}$. For four other samples, of composition $Gd_{76.5}Lu_{23.5}$, $Gd_{76.3}Lu_{23.7}$, $Gd_{75.7}Lu_{24.3}$, and $Gd_{75.3}Lu_{24.7}$, only C_{33} and α_{33} were measured. The indices 33 correspond to a longitudinal wave propagated parallel to the *c*-axis; 44, in this case, to a transverse wave propagated parallel to the *c*-axis with the polarization vector in the basal plane; and 11 to a longitudinal wave propagated across the basal plane. C_{44} can also be derived from the velocity of a transverse wave propagated parallel to the basal plane with the polarization vector parallel to the *c*-axis.

The C_{33}-mode offers the strongest coupling to the magnetic structures displayed. The addition of symmetry elements into the magnetic structure will soften C_{33} and critical fluctuations will cause singularities in α_{33}. In addition, both C_{33} and α_{33} will be affected by some magnetic domain structures.

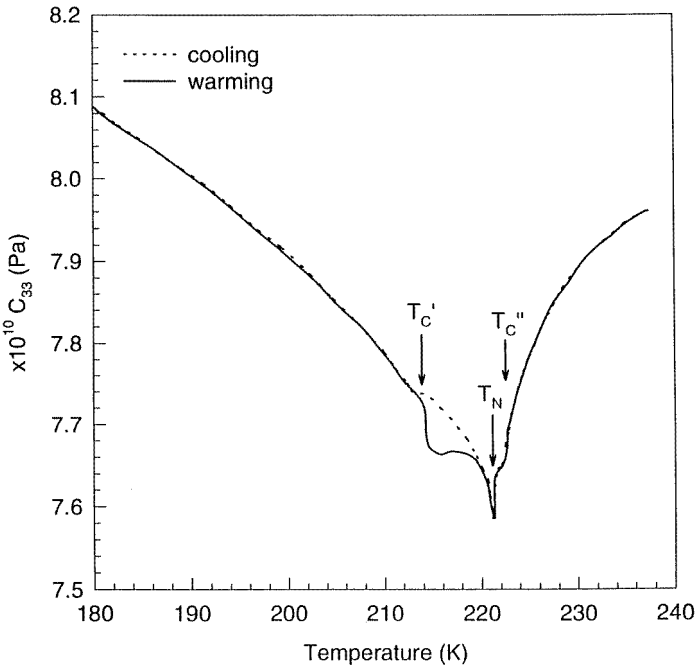

Figure 1. C_{33} versus temperature for $Gd_{76.0}Lu_{24.0}$.

The C_{33}-data for $Gd_{76.0}Lu_{24.0}$ are shown in figure 1. A clear transition is evident at 221 K associated with a sharp minimum; however, a small inflection at 222.5 K discloses

a higher initial ordering temperature. On cooling, a small inflection at 212 K provides evidence of a third transition. From this temperature down to 4 K the elastic constant evolves smoothly. On warming, dramatic hysteresis is observed with C_{33} softening with respect to the data collected on cooling, and not recovering until 220 K is reached. There is no hysteresis outside error limits in either of the higher-temperature transitions.

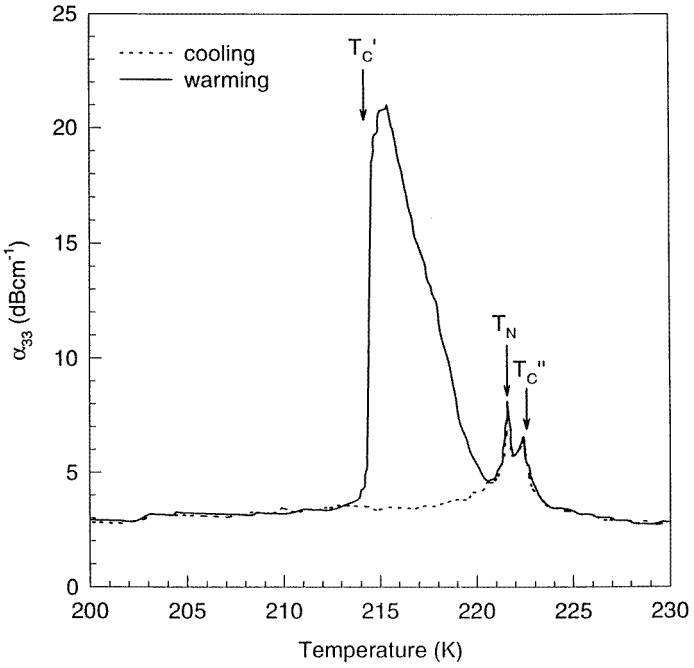

Figure 2. α_{33} versus temperature for $Gd_{76.0}Lu_{24.0}$.

Likewise, the attenuation data (figure 2) show evidence of transitions at 222.5 K and 221 K, and dramatic hysteresis in the region 221 K to 212 K.

These data agree well with the anticipated structure. Because the ferro I phase arises from weak exchange coupling it will only couple weakly to the elastic constant—hence the small inflection in C_{33} at the initial ordering transition. However, critical fluctuations are sufficient to reveal a clearly visible peak in α_{33}. The minimum in C_{33} reveals the Néel temperature. Hereinafter we will refer to the ferro I, ferro II and HAF upper ordering temperatures as T_c'', T_c' and T_N respectively. The hysteresis in both C_{33} and α_{33} is characteristic of a helical antiferromagnetic phase and arises from differences in the domain structure [13]: in the helical antiferromagnetic region, domains are chiral. On cooling from the paramagnetic region the domains are randomly seeded on crystal imperfections and will grow as mosaic blocks. On warming from a magnetic structure with a component of the magnetization in the basal plane, into the helical antiferromagnetic phase, domains form as stripes perpendicular to the *c*-axis. The walls between two domains of opposing chirality are a ferromagnetic region, estimated to be some 100 layers wide in Gd–Y. This effect has been elegantly demonstrated by neutron topography [14]. The passage of the ultrasonic wave leaves the random domains unaffected; however, as it travels through the striped domains the helical turn angle is altered [15]. This in itself is not the mechanism which dissipates the majority of the ultrasonic energy, although it does provide a small contribution to the

attenuation that is turn angle, and hence temperature, independent. At the domain wall–domain interface, a delicate interplay between the domain wall energy and the exchange interactions takes place. At large turn angles the interface is quite distinct; however, at small turn angles only a small change in the helical turn angle is required to bring the spins that are close to the domain wall into alignment with the ferromagnetically aligned spins in the domain wall, thus increasing the thickness of the domain wall. Consequently, the passage of the ultrasonic wave causes a breathing of the domain wall which dissipates energy. This effect is considerably stronger at small turn angles than at higher turn angles [16].

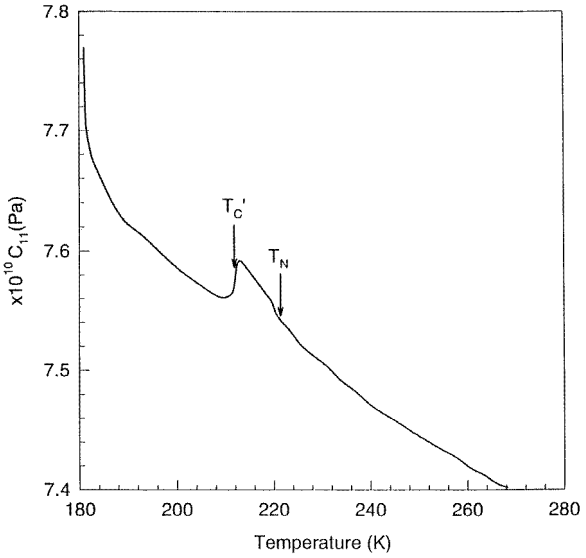

Figure 3. C_{11} versus temperature for $Gd_{76.0}Lu_{24.0}$.

C_{44} shows a very modest inflection at T_N, but no coupling to either T_c' or T_c''. C_{11} (figure 3) shows an inflection at T_N; however, at T_c' the magnetostrictive contraction of the *c*-axis of the crystal was sufficient to break the bond between the sample and the transducer despite the use of a variety of couplants.

The behaviour of C_{33} and α_{33} for $Gd_{76.2}Lu_{23.7}$ and $Gd_{75.7}Lu_{24.3}$ samples is very similar to that for $Gd_{76.0}Lu_{24.0}$ albeit with changes in the transition temperatures. C_{33} and α_{33} for $Gd_{76.5}Lu_{24.0}$ show no evidence for a HAF region, while at the other end of the composition range studied, $Gd_{75.3}Lu_{24.7}$ does not appear to display a ferro I phase.

On the basis of these measurements and in the light of the earlier work by Legvold *et al* [17] and Ito *et al* [18] we are able to make some assumptions about the magnetic structure observed in the Gd–Lu phase diagram. Our phase diagram is shown in figure 5 and is very similar to that of Gd–Y. Ito *et al* have observed a ferro I phase in a $Gd_{80}Lu_{20}$ single crystal, which was stable over a temperature range of only 2 K.

3.2. Neutron scattering measurements

On the basis of this phase diagram we were able to direct the focus of our neutron diffraction measurements to the features of the phase diagram that we anticipated to be of most interest: the ferro II–HAF transition and the ferro I region.

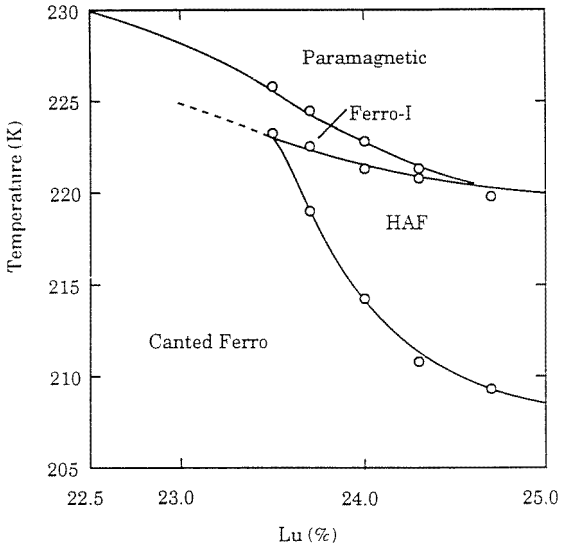

Figure 4. A partial magnetic phase diagram for the Gd–Lu alloy system.

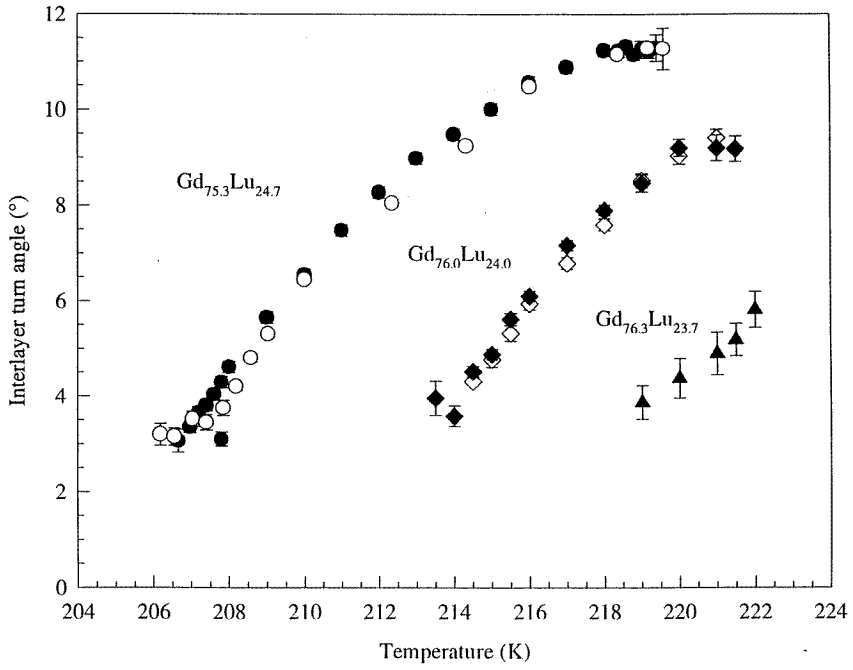

Figure 5. The interlayer turn angle, ω, versus temperature. The filled symbols represent data collected whilst cooling.

In the region of the phase diagram where the magnetic structure is anticipated to be that of a HAF satellite, reflections were only observed at $(h, k, l \pm q)$, characteristic of a

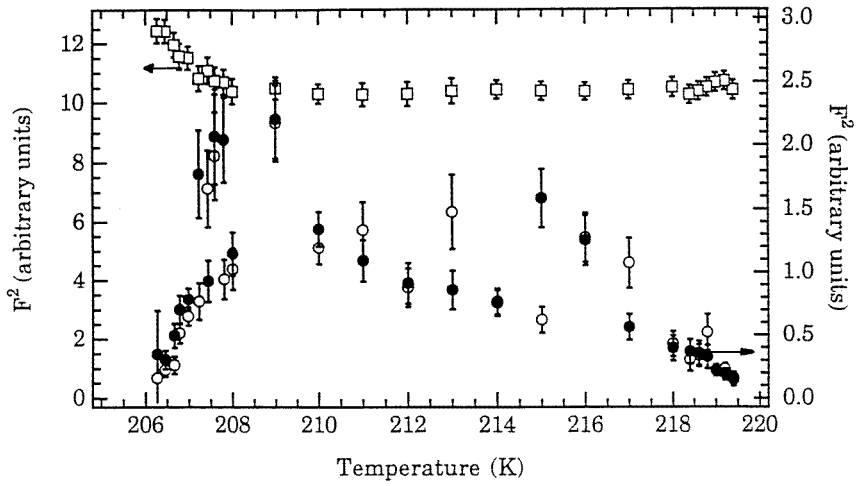

Figure 6. The intensity of the (101) peak (squares and left-hand axis) and the $(101)^+$ and $(101)^-$ satellites (filled and open circles respectively) versus temperature for $Gd_{75.3}Lu_{24.7}$.

basal-plane helix with propagation vector $q = \omega/\pi$, where ω is the interlayer turn angle of the helix. The relative intensities of basal-plane and out-of-plane reflections confirmed that the moment was confined to the basal plane. Thus temperature scans across the helical region revealed the thermal evolution of ω as shown in figure 5. Clearly, in all three measured cases, the turn angle decreases continuously towards zero at T_c', and shows no significant thermal hysteresis. The turn angle was measured down to 3° before the intensity of the satellite reflections became immeasurably small. A study of the intensity of the satellite reflections (figure 6) shows an increase in intensity of the satellites as the moment develops; however, within 2 K of the transition the intensity starts to decrease and additional scattering is seen on the nuclear peak showing the development of a ferromagnetic moment. The absorption cross section of these Gd–Lu alloys is such that we may be preferentially viewing surface effects rather than the behaviour of the bulk of the specimen; however, these data are consistent with the growth of ferromagnetic domains at the expense of HAF domains.

Returning to our model of the domain structure in the HAF phase which explains the hysteresis in the ultrasonic attenuation we could expect to see hysteresis in the widths of the satellite peaks, reflecting differences in the correlation lengths for the two different domain structures. Figure 7 shows the HWHM of the satellite peaks of the type $(1, 0, 1 \pm q)$ versus temperature for $Gd_{75.3}Lu_{24.7}$ on both warming and cooling. The nuclear peak width is plotted for reference. It is clear that at temperatures near T_c', where the turn angle is small, the satellite width is appreciably greater on warming from the ferro II phase than on cooling, consistent with small domain walls growing out of domain walls in the canted ferromagnetic phase.

The spontaneous magnetization can be calculated from the ratio of the magnetic scattering intensity to the nuclear scattering intensity as follows:

$$\frac{I_{mag}}{I_{nuc}} = \frac{F_{mag}^2}{F_{nuc}^2} = \frac{c\gamma r_0^2 f(\kappa)^2 M(\boldsymbol{q})^2}{4b^2}$$

where c is the concentration of magnetic atoms, γ is the magnetic moment of the neutron,

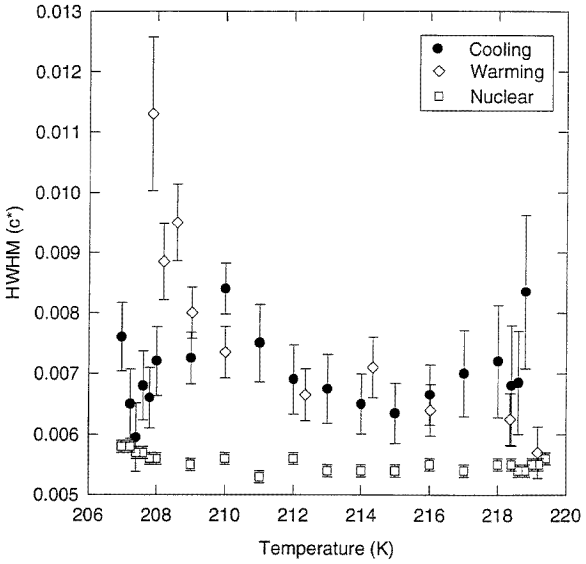

Figure 7. The HWHM of the (101) nuclear peak and the (1, 0, 1±q) satellites versus temperature for $Gd_{75.3}Lu_{24.7}$.

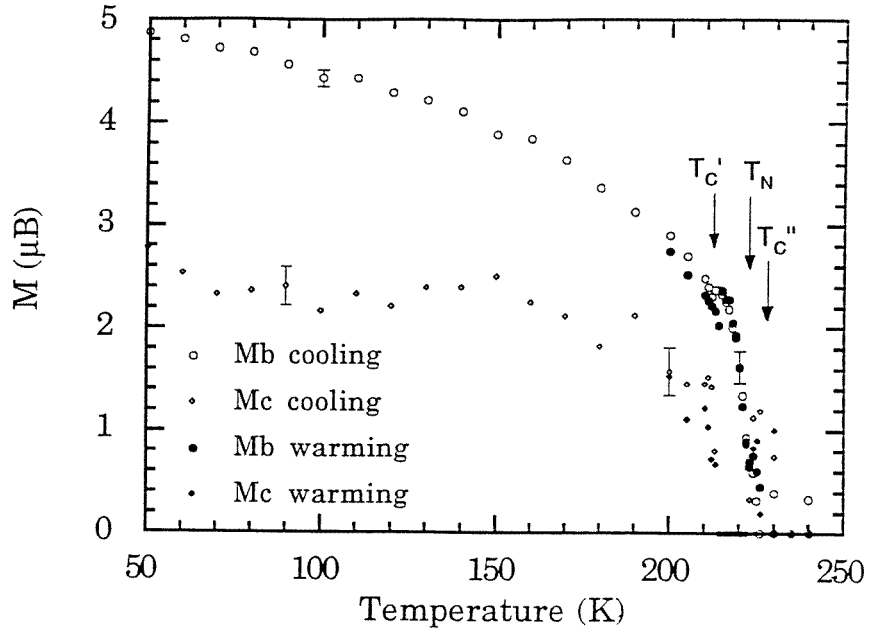

Figure 8. M_b and M_c versus temperature for $Gd_{76.0}Lu_{24.0}$.

r_0 is the classical radius of the electron, b is the mean nuclear scattering length, $M(\boldsymbol{q})$ is the spontaneous magnetization and $f(\kappa)$ is the magnetic form factor. The magnetic form factors used in this case were those calculated by Stassis *et al* [19]. The basal-plane

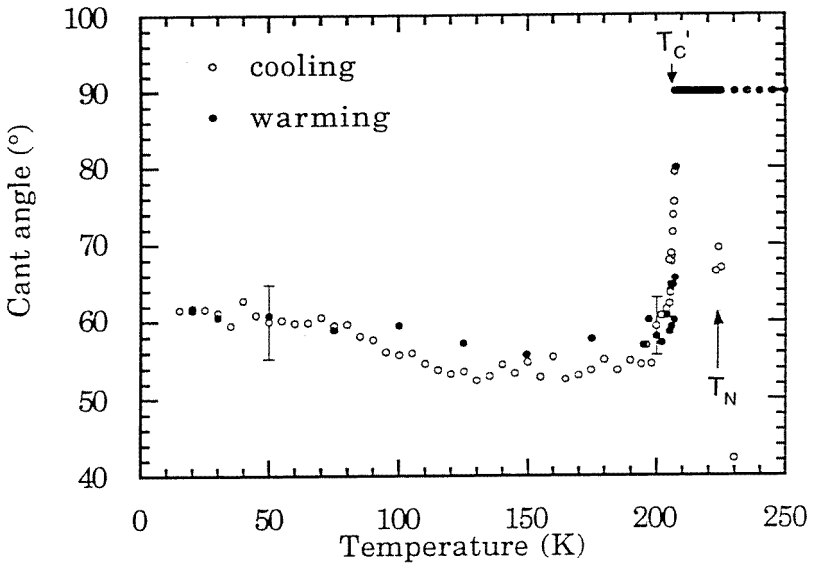

Figure 9. The cant angle versus temperature for $Gd_{75.3}Lu_{24.7}$.

component of the magnetization can be determined solely from reflections of the type (00*l*) whereas components to the magnetization along the *c*-axis and in the basal plane contribute to reflections of the (*hk*0) type thus:

$$M_{(002)}(\boldsymbol{q})^2 = M_b^2$$

$$M_{(100)}(\boldsymbol{q})^2 = M_c^2 + \frac{M_b^2}{2}.$$

The components M_c and M_b determined in this manner have been plotted for $Gd_{76}Lu_{24}$ (figure 8). The three phase transitions determined by our ultrasound measurements can be identified, although the limited temperature range of the ferro I region and the small moment hampers a thorough study of this phase. From these data the ferromagnetic cant angle has been calculated and plotted (figure 9). As the temperature is reduced a moment develops along the *c*-axis, consistent with a ferro I phase, before collapsing into the basal plane in the HAF phase. At T_c' the moments rise rapidly away from the basal plane to adopt a canted ferromagnetic structure with a cant angle of approximately 60° to the *c*-axis. There is no evidence of an intermediate basal-plane ferromagnetic phase. Extensive scans across full Brillouin zones in the canted ferromagnetic region confirmed that there is no scattering other than scattering on the nuclear Bragg peaks consistent with the canted ferromagnetic structure.

4. Conclusions

Ultrasonic and neutron scattering measurements have been used to determine the temperature–concentration phase diagram of Gd–Lu in the multicritical region. The phase diagram that we have produced is very similar to that of Gd–Y, including the observation of two multicritical points. The ferro I region is considerably reduced in Gd–Lu compared to Gd–Y in terms of both temperature and diluent concentration, and as a consequence

we have been unable to extend studies of this magnetic structure. In the case of Gd–Y the tricritical points occur at Y concentrations of 33% and 29.5%, whereas in the case of Gd–Lu the same tricritical points occur at Lu concentrations of 24.7% and 23.5%. The HAF–ferro II transition has been studied and, again, the observed behaviour is almost identical to that observed in Gd–Y. The ultrasound and neutron scattering data support a model for the transition which involves the development of HAF domains out of domain walls in the ferro II phase, leading to a small region where the two phases coexist. Similar behaviour has been observed by neutron topography at the transition from a HAF structure to a basal-plane ferromagnetic structure in terbium. However, our data show no evidence of an intermediate basal plane ferromagnetic structure in Gd–Lu.

References

[1] Cable J W and Koehler W C 1982 *J. Appl. Phys.* **53** 1904
[2] Jensen J and Mackintosh A R 1991 *Rare Earth Magnetism, Structures and Excitations* (Oxford: Oxford Science)
[3] Kaino K and Kasuya J 1981 *J. Phys. F: Met. Phys.* **11** 88 3
[4] Williams R W and Mackintosh A R 1987 *Phys. Rev.* B **36** 3809
[5] Liu S H, Gupta R R and Sinha S K 1971 *Phys. Rev.* B **4** 1100
[6] Bates S, Palmer S B, Sousa J B, McIntyre G J, Fort D, Legvold S, Beaudry B J and Koehler W C 1985 *Phys. Rev. Lett.* **55** 27 2968
[7] Legvold S, Ito T and Beaudry B J 1980 *Phys. Rev. Lett.* **45** 15 1275
[8] Bates S, McIntyre G J, Palmer S B and Sousa J B 1987 *J. Phys. F: Met. Phys.* **17** 1973
[9] Melville R J, Bates S, McIntyre G J, Sousa J B and Palmer S B 1988 *Europhys. Lett.* **6** 725
[10] Eccleston R S, Griffiths A R, Vrtis M L, McIntyre G J, Fort D and Palmer S B 1991 *Physica* B **174** 33–8
[11] Fort D 1991 *J. Alloys Compounds* **177** 31–47
[12] Salgeiro da Silva, Eccleston R S, Bessa Sousa J and Palmer S B 1992 *Ultrasonics* **30** 347
[13] Palmer S B 1975 *J. Phys. F: Met. Phys.* **5** 2370
[14] Baruchel J, Palmer S B and Schlenker M 1981 *J. Physique* **42** 1279
[15] Tachiki M, Levy M, Kagiwada R and Lee M C 1968 *Phys. Rev. Lett.* **21** 1193
[16] Bates S 1985 *PhD Thesis* University of Hull
[17] Legvold S, Harmon B N, Beaudry B J, Bugardt P, Younkin D R and White H W 1977 *Phys. Rev.* **16** 4986
[18] Ito T, Oka M, Legvold S and Beaudry B J 1984 *Phys. Rev.* B **29** 6276
[19] Stassis C, Deckmand H W, Harmon B N, Desclaux J P and Freeman A J 1977 *Phys. Rev.* B **15** 369